

Boundary critical phenomena of the random transverse Ising model in $D \geq 2$ dimensions

István A. Kovács^{1,*} and Ferenc Iglói^{1,2,†}

¹*Wigner Research Centre, Institute for Solid State Physics and Optics, H-1525 Budapest, P.O.Box 49, Hungary*

²*Institute of Theoretical Physics, Szeged University, H-6720 Szeged, Hungary*

(Dated: December 3, 2024)

Using the strong disorder renormalization group method we study numerically the critical behavior of the random transverse Ising model at a free surface, at a corner and at an edge in $D = 2, 3$ and 4-dimensional lattices. The surface magnetization exponents are found to be: $x_s = 1.60(2), 2.65(15)$ and $3.7(1)$ in $D = 2, 3$ and 4, respectively, which do not depend on the form of disorder. We have also studied critical magnetization profiles in slab, pyramid and wedge geometries with fixed-free boundary conditions and analyzed their scaling behavior.

I. INTRODUCTION

The quantum Ising model with random couplings and/or with random transverse fields (RTIM) is the prototype of disordered quantum magnets having discrete symmetry. This model has a zero-temperature quantum phase transition, the properties of which have been studied by a special strong disorder renormalization group (SDRG) method¹. In this method the strongest local terms of the Hamiltonian are successively eliminated and at the same time new terms are generated perturbatively between remaining degrees of freedom². In one dimension (1D) where the topology of the lattice stays invariant under the transformation the SDRG equations have been solved analytically in the vicinity of the quantum critical point³. In this case the phase transition is shown to be controlled by a so called infinite disorder fixed point⁴ (IDFP), in which disorder fluctuations are completely dominant over quantum fluctuations and therefore the renormalization steps are asymptotically exact for large scales. Indeed the SDRG results in 1D are consistent with findings of other analytical^{5,6} and numerical methods⁷⁻⁹.

In higher dimensional lattices the topology of the lattice is changed during the SDRG steps, therefore the SDRG method has to be implemented numerically. The first numerical calculations have been performed in 2D¹⁰⁻¹⁵ and more recently an efficient numerical algorithm¹⁶⁻¹⁸ of the present authors made possible to extend the calculations¹⁷⁻²⁰ to 3D and 4D, as well as to Erdős-Rényi random graphs, which are infinite dimensional lattices. In all dimensions the phase transition is found to be controlled by an IDFP, which justifies that the SDRG method provides asymptotically exact results for large systems in higher dimensions, too. Quantum Monte Carlo simulations for the 2D RTIM are consistent with the SDRG results²¹. Similarly, simulation results for the random contact process^{22,23} - which is expected to be in the same universality class²⁴ as the RTIM - are in agreement with the SDRG results in 2D and in 3D.

In $D > 1$ dimensions during the SDRG iterations a large number of new couplings are generated between remote sites, which makes the numerical implementation of the method rather cumbersome. To avoid this problem

approximation methods have been developed and applied to the RTIM²⁵⁻³¹. One of those²⁵ is based on the quantum cavity approach³², which is found to reproduce some of the exact results in 1D. However in the Bethe lattice with an effective dimensionality of $D_{\text{eff}} = 2$ the method has predicted conventional random critical behavior instead of IDFP scaling. The generalized version of the quantum cavity method for higher dimensional lattices, the so called non-linear transfer approach²⁷, however has lead to IDFP behavior for $D \geq 2$. Also approximate renormalization group schemes have been suggested²⁸⁻³¹, during which the order of the RG steps is changed in such a way that the proliferation of new couplings is avoided. These methods have reproduced some exact 1D results and also provide IDFP behavior for $D \geq 2$, in agreement with the standard SDRG method.

Most of the results about the critical behavior of the RTIM have been calculated for bulk quantities. For example the order-parameter of the RTIM is the average magnetization and its value in the bulk, m_b , has the scaling behavior $m_b \sim L^{-x}$, where L is the linear size of the system and x is the scaling exponent of the bulk magnetization. Real systems, however, have finite extent and they are limited by boundaries. At a free surface the scaling behavior of the average surface magnetization, m_s , involves a new exponent³³⁻³⁵, x_s . Due to missing bonds at the surface there is weaker order, therefore generally $x_s > x$. For the 1D RTIM several properties of the surface magnetization (the distribution function, average and typical behavior, etc) is exactly known^{3,5,9,36}. For example the surface scaling exponent, $x_s = 1/2$, is related to the persistence properties of 1D random walks⁹.

For higher dimensional RTIM less attention is paid to the calculation of the surface magnetization: we are aware of one recent work²⁷, in which the surface magnetization exponent has been calculated by the non-linear transfer approach. The obtained values are $x_s = 1.2$ and 1.34 , in 2D and 3D, respectively, which are to be compared with the SDRG results for the bulk magnetization exponent¹⁶⁻¹⁸: $x = 0.98$ and 1.84 , in 2D and 3D, respectively. Since in 3D the surface magnetization exponent of the non-linear transfer approach is smaller, than the expected correct value of the bulk magnetization expo-

ment we conclude that the non-linear transfer approach underestimates the values of x_s . Therefore there is a necessity to obtain more accurate estimates for the surface critical properties of the RTIM.

In this paper we study the boundary critical behavior of the RTIM in higher dimensional systems for $D = 2, 3$ and 4 by the SDRG method. In the calculation we use the numerical algorithm, which has been developed in Refs.^{17,18} and has been used to study the bulk critical behavior of the systems. Besides the surface magnetization exponent, x_s , we calculate local magnetization exponents³⁷, which are associated with corners (in 2D and 3D) as well as with edges (in 3D). We also calculate critical magnetization profiles, when spins are fixed at some surfaces of the system and study their scaling properties.

The structure of the paper is the following. The essence of the SDRG method and its application to the calculation of the boundary magnetization is described in Sec.II. Our results for 2D, 3D and 4D lattices are presented in Sec.III and discussed in the final section.

II. SDRG CALCULATION OF THE LOCAL MAGNETIZATION

Here we consider the boundary critical properties of the RTIM defined by the Hamiltonian:

$$\mathcal{H} = - \sum_{ij} J_{ij} \sigma_i^x \sigma_j^x - \sum_i h_i \sigma_i^z \quad (1)$$

in terms of the $\sigma_i^{x,z}$ Pauli operators at site i of a D -dimensional cubic lattice. The $J_{ij} > 0$ nearest-neighbor couplings and the $h_i > 0$ transverse fields are independent random numbers taken from the distributions $p(J)$ and $q(h)$, respectively. In this paper we have used two different disorder distributions, like in Refs.¹⁶⁻¹⁸. In both cases the couplings are taken from a uniform distribution: $p(J) = \Theta(J)\Theta(1 - J)$, where $\Theta(x)$ is the Heaviside step-function. For the *box-h model* the transverse fields have a box-like distribution $q(h) = \frac{1}{h_b} \Theta(h)\Theta(h_b - h)$, whereas for the *fixed-h model* the transverse fields are constant: $q(h) = \delta(h - h_f)$.

In the calculations of different local magnetizations (surface, edge and corner) we have used different finite geometries, in which fixed spin boundary conditions (b.c.) have been used at given planes and the magnetization profile, m_l , is measured perpendicular to the fixed planes. (These are located at $l = 1$, thus $m_1 = 1$). For the *surface magnetization* a slab of size $L \times N^{D-1}$ ($L < N$) is used, and in the short direction we use fixed-free b.c., while in the other $(D - 1)$ -directions periodic b.c. is applied. The surface magnetization is given by $m_s = m_{l=L}$, which scales at the critical point as $m_s \sim L^{-x_s}$.

The *corner magnetization* is measured at the free corner of a cube, so that the system has a pyramid shape and the spins at the base of the pyramid are fixed, while at other surfaces free b.c.-s are used. The magnetization

profile, m_l is measured between the base ($l = 1$) and the corner ($l = L_c = \frac{\sqrt{D}}{2}L$), and the corner magnetization is given by $m_c = m_{l=L_c}$. This scales at the critical point as $m_c \sim L^{-x_c}$ with the corner exponent, x_c .

Edge magnetization is calculated in 3D at the free edge of length N of a square column of size $L \times L \times N$, $L < N$. The square column is cut at the square diagonal plane, thus have the shape of a wedge, and the spins at the base of the wedge are fixed. In the long direction periodic b.c. is used, while at the other two symmetric surfaces free b.c. is applied. The magnetization profile, m_l is measured between the base of the wedge ($l = 1$) and the free edge ($l = L_e = \frac{\sqrt{2}}{2}L$). m_l is translationally invariant along the long direction and the edge magnetization is given by $m_e = m_{l=L_e}$. This scales at the critical point as $m_e \sim L^{-x_e}$, with the edge exponent, x_e .

To calculate the local magnetization in the different geometries we have used the SDRG method, which is an iterative procedure working in the energy space. At each step the largest local term of the Hamiltonian, either a coupling, J_{ij} , or a transverse field, h_i , is decimated and new terms are generated between the remaining sites in a perturbation calculation. For coupling decimation the two sites, i and j with original magnetic moments, μ_i and μ_j , are merged to a new cluster with an effective moment $\mu'_{ij} = \mu_i + \mu_j$, which is placed in an effective transverse field of strength: $h'_{ij} = h_i h_j / J_{ij}$. In transverse field decimation the site i is eliminated and its nearest-neighbor sites, say j and k will be connected by an effective coupling: $J'_{jk} = \max\{J_{ji}J_{ik}/h_i, J_{jk}\}$. In this last step the so called maximum rule is applied, the use of which is justified at an IDFP.

We apply the numerical algorithm of the SDRG method in Refs.^{17,18}, which has been used to locate the critical point of the system (for the two forms of the disorder) and to calculate the bulk critical exponents at the IDFP for different dimensions, $D = 2, 3$ and 4 (which are disorder independent and listed in Table II). To calculate the critical magnetization profile, m_l , we renormalize the system up to the last effective site and consider the effective cluster, \mathcal{C} , which contains the fixed sites at $l = 1$. If the system has an IDFP, then all spins of \mathcal{C} are strongly correlated: in leading order all these spins point to the same direction as at $l = 1$, whereas other sites (not contained in \mathcal{C}) have negligible contribution to the longitudinal magnetization. Let us denote by n_l the number of sites in \mathcal{C} at position l and the number of equivalent sites by \tilde{n} (it is N^{d-1} , N and 1 in the slab, wedge and pyramid geometry, respectively). The average value of the local magnetization is then given by: $m_l = [n_l/\tilde{n}]_{\text{av}}$, where $[\dots]_{\text{av}}$ stands for the average over disorder realizations.

At the critical point the asymptotic form of the magnetization profile is given by scaling considerations. According to Fisher and de Gennes³⁸ the decay of the magnetization from the fixed surface is given by:

$$m_l \sim l^{-x_b}, \quad x = x_b, \quad 1 \ll l \ll L, \quad (2)$$

thus it includes the bulk magnetization exponent. Close

to the free endpoint (surface, corner or edge) the magnetization profile has a different power-law decay³³:

$$m_{l'} \sim (l')^{x_{ab}}, \quad 1 \ll l' = L_\alpha - l + 1 \ll L_\alpha, \quad (3)$$

with $x_{ab} = x_\alpha - x$ and α relates to the type of endpoint: s , c or e (and $L_s \equiv L$). These relations will be used to obtain independent estimates for the local magnetization exponents. The two scaling relations in Eqs.(2) and (3) can be incorporated into an interpolation formula:

$$m_l = \frac{A}{L^x} [\sin(\pi\lambda)]^x [\cos(\pi\lambda/2)]^{x_\alpha}, \quad (4)$$

with $\lambda = \frac{l}{L_\alpha}$. This relation is exact for 1D conformally invariant quantum systems³⁹. Although the RTIM is not conformally invariant, in 1D Eq.(4) is found to be an excellent approximation^{8,40}. In the following in the slab geometry ($\alpha = s$) we shall check the accuracy of Eq.(4) in higher dimensions, too.

III. RESULTS

We have calculated the magnetization profiles in the three geometries described in Sec.II in different dimensions: $2 \leq D \leq 4$ by the SDRG method using two different forms of disorder. The largest sizes of the systems, the typical aspect ratios of slabs and wedges as well as the typical number of disorder realizations are collected in Table I. Since only a small fraction of samples contains such a correlation cluster, \mathcal{C} , which have also sites at the free extremity of the system (surface, edge or corner) one should consider a large number of realizations. For surfaces and edges in a given sample there are several end-point positions, for which we perform the averages. For corners, however, there is just one end-point in a sample, therefore one should take even larger number of realizations. In the following we present our numerical results obtained in different dimensions.

TABLE I: Details of the numerical calculation of the local magnetization. L_{\max} : largest linear size; N/L : typical aspect ratio; $N^\#$: typical number of realizations.

	slab			pyramid		wedge		
	L_{\max}	N/L	$N^\#$	L_{\max}	$N^\#$	L_{\max}	N/L	$N^\#$
2D	512	4.	10^6	256	10^7			
3D	64	2.	10^6	64	10^8	64	2.	10^7
4D	32	1.5	10^5					

A. Calculations in 2D

1. Surface magnetization

The magnetization profiles in the slab geometry calculated by the two types of disorder are shown in Fig.1 as

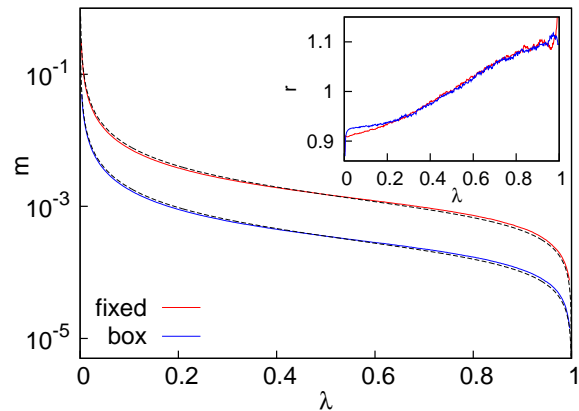


FIG. 1: (Color online) Magnetization profiles in 2D in the slab geometry for fixed-free b.c.-s in a system of width $L = 512$ for box- h and fixed- h randomness. The interpolation formula in Eq.(4) is represented by dashed lines. In the inset the ratio of the magnetization profile and the interpolation formula in Eq.(4) is shown for $x = 0.982$, $x_s = 1.6$, $A_{\text{fixed}} = 1.20$ and $A_{\text{box}} = 0.282$.

a function of the relative position: $\lambda = l/L$, see Eq.(4). Here we use a finite-size shift of $l_0 = \mathcal{O}(1)$ at the boundaries. As already observed in the calculation of the bulk magnetization the typical correlation clusters for fixed- h disorder contain approximately 6-times more sites, than for box- h disorder. As a consequence the magnetization profiles are also comparatively larger for fixed- h disorder. As seen in Fig.1 the magnetization is monotonously decreasing and the variation is very fast near the two end-points, which are then analyzed in log-log plots in Figs.2 and 3, respectively.

Close to the fixed boundary the magnetization profiles are shown in Fig.2, together with the similar profiles in the pyramid geometry, which will be analyzed in Sec.III A 2. The magnetization profiles for the two disorder have the same power-law decay and the decay exponent is estimated from the largest systems as $x_b = 0.98(1)$. This is to be compared with the value of the bulk magnetization exponent $x = 0.982(15)$, which has been calculated in Ref.¹⁶ by finite size scaling. We can thus conclude that the Fisher-de Gennes scaling prediction in Eq.(2) is well satisfied.

Also at the free-boundary the profiles have a power-law variation (see Fig.3) and the corresponding exponent is estimated from the largest system as: $x_{sb} = 0.65(2)$. We have also calculated the surface magnetization exponent, x_s , from the finite-size scaling behavior of the surface magnetization, m_s . Two-point estimates for x_s are presented in the inset of Fig. 3, which have the same limiting value for large L for the two type of disorder, which is presented in Table II. Comparing x_{sb} with $x_s - x$ we can conclude that the scaling prediction in Eq.(3) is satisfied.

We have also checked the accuracy of the interpolation formula in Eq.(4) and in the inset of Fig.1 we have plotted

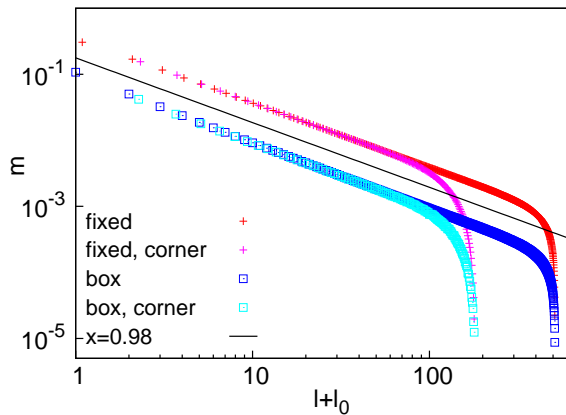


FIG. 2: (Color online) Magnetization profiles near the fixed boundary in 2D for the slab and the pyramid geometries for the fixed- h and box- h randomness with $L = 512$ and 256 , respectively. In all cases the decay is characterized by the same exponent, $x_b = 0.98(1)$, which according to the Fisher-de Gennes result in Eq.(2) is equivalent to the bulk magnetization exponent, see Table II.

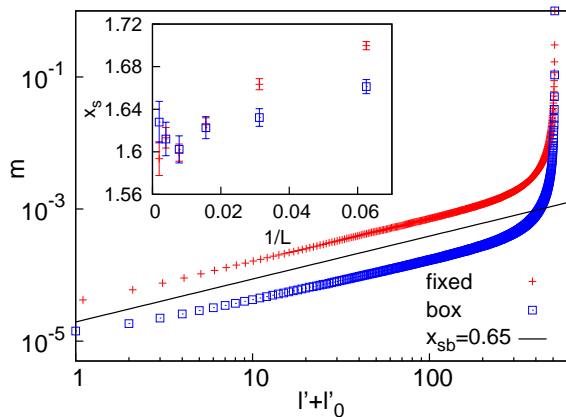


FIG. 3: (Color online) Magnetization profiles near the free boundary in 2D for the slab geometry for the two type of randomness with $L = 512$. In both cases the decay is characterized by the exponent, $x_{sb} = 0.65(2)$. In the inset the finite-size estimates for the surface magnetization exponent are presented. The extrapolated (disorder independent) value is given in Table II.

the ratio of the measured profile and the interpolation formula, in which the exponents in Table II have been used. As seen in this figure the interpolation formula represents a good approximation, but the agreement is not perfect, the largest discrepancy is about 10%.

2. Corner magnetization

The calculations are performed in the pyramid geometry and the critical magnetization profile close to the fixed plane is shown in Fig.1 in a log-log plot for the two different initial disorder. As discussed in Sec.III A 1 in this figure also the profiles in the slab geometry are presented and the two types of profiles are very close to each other: they are indistinguishable within the error of the calculation. Thus in agreement with scaling theory the decay of the profile in the pyramid geometry is in a power-law form with a decay exponent, $x_b = x$. The magnetization profile at the other end, i.e. starting from the corner is shown in Fig.4 and the corresponding decay exponent of the magnetization, x_{cb} , is presented in Table II.

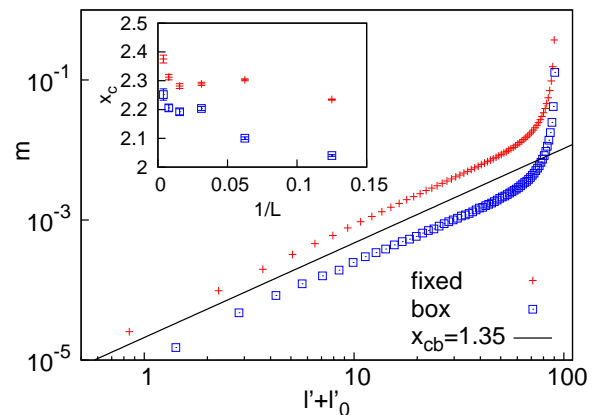


FIG. 4: (Color online) Magnetization profiles in the pyramid geometry near the corner in 2D for the two type of randomness with $L = 256$. In both cases the decay is characterized by the exponent, $x_{cb} = 1.35(10)$. In the inset the finite-size estimates for the corner magnetization exponent are presented. The extrapolated (disorder independent) value is given in Table II.

From finite-size scaling the corner magnetization exponent, x_c , is calculated by two-point fit and the effective, size-dependent exponents are presented in the inset of Fig.4 for the two different type of disorder. The extrapolated value which is disorder independent is given in Table II.

B. Calculations in 3D

1. Surface magnetization

The magnetization profiles in the slab geometry are shown in Fig. 5 for the two types of disorder. Close to the fixed boundary the exponent associated to the decay of the profile is estimated as $x_b = 1.855(20)$ which agrees with the finite-size estimate of the bulk magnetization

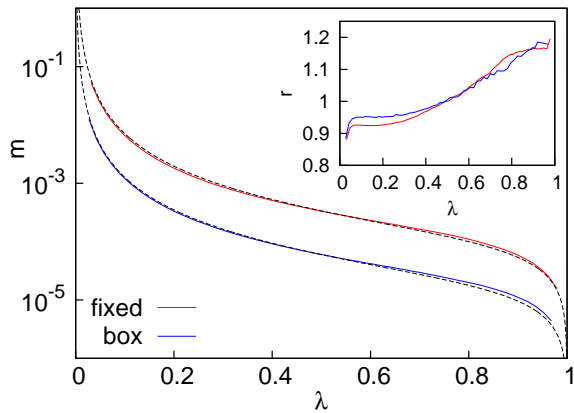


FIG. 5: (Color online) Magnetization profiles in 3D in the slab geometry for fixed-free b.c.-s in a system of width $L = 64$ for box- h and fixed- h randomness. The interpolation formula in Eq.(4) is represented by dashed lines. In the inset the ratio of the magnetization profile and the interpolation formula in Eq.(4) is shown for $x = 1.84$, $x_s = 2.65$, $A_{\text{fixed}} = 1.78$ and $A_{\text{box}} = 0.316$.

exponent, see Table II. Near the free surface the profiles for the two types of disorder are shown in Fig. 6 and the estimated decay exponent, x_{sb} , is presented in Table II.

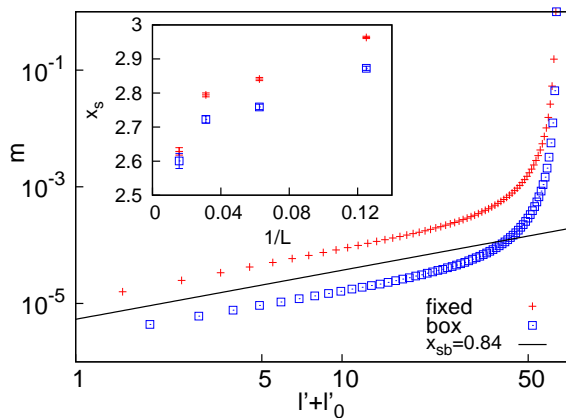


FIG. 6: (Color online) Magnetization profiles near the free boundary in 3D for the slab geometry for the two types of randomness with $L = 64$. In both cases the decay is characterized by the exponent, $x_{sb} = 0.84(7)$. In the inset the finite-size estimates for the surface magnetization exponent are presented. The extrapolated (disorder independent) value is given in Table II.

The surface magnetization exponent is estimated through finite-size scaling and the effective, size-dependent values are shown in the inset of Fig. 6 for the two types of disorder. The extrapolated exponent is disorder independent and given in Table II. We conclude that the scaling relation in Eq.(3) is satisfied within the

error of the calculation.

We have checked the accuracy of the interpolation formula in Eq.(4) and the ratio of the measured profile and the interpolation formula is shown in the inset of Fig. 5. Also in this case Eq.(4) is a good approximation, the maximal discrepancy is somewhat larger, than in the 2D case, see in Fig. 1.

2. Edge magnetization

We have measured the magnetization profile in the wedge geometry and here we analyze its behavior close to the free edge, see Fig. 7.

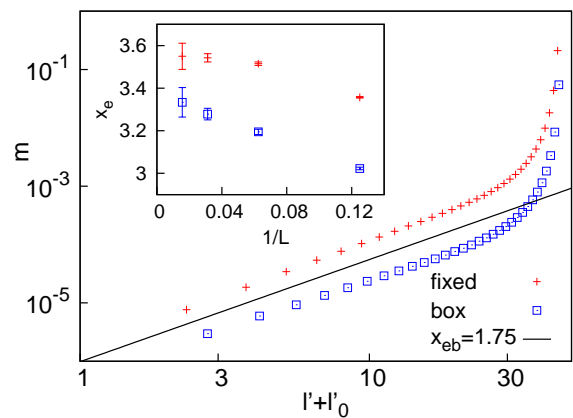


FIG. 7: (Color online) Magnetization profiles near the free edge in 3D in the wedge geometry for the two type of randomness with $L = 64$. In both cases the decay is characterized by the exponent, $x_{eb} = 1.75(15)$. In the inset the finite-size estimates for the edge magnetization exponent are presented. The extrapolated (disorder independent) value is given in Table II.

The estimated decay exponent, x_{eb} , is presented in Table II together with the extrapolated value of the edge exponent, x_e , for which the finite-size estimates are shown in the inset of Fig. 7. In this case, too the scaling relation in Eq.(3) is satisfied.

3. Corner magnetization

We close our study in 3D by calculating the magnetization profile in the pyramid geometry: the result is shown in Fig. 8 close to the free corner. (In the inset finite-size estimates of the corner exponent are presented.) Estimates of the decay exponent, x_{cb} , and the corner exponent, x_c , are presented in Table II, which satisfy the scaling relation in Eq.(3).

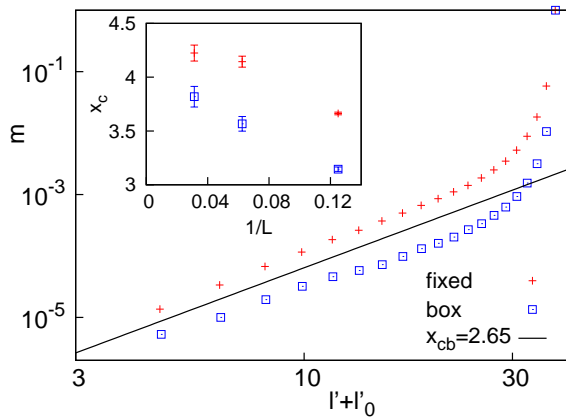


FIG. 8: (Color online) Magnetization profiles near the free corner in 3D in the pyramid geometry for the two type of randomness with $L = 64$. In both cases the decay is characterized by the exponent, $x_{cb} = 2.65(25)$. In the inset the finite-size estimates for the edge magnetization exponent are presented up to $L = 32$. The extrapolated (disorder independent) value is given in Table II.

C. Calculations in 4D

In 4D the available system sizes are limited, see Table I, therefore we could only study the magnetization profile in the slab geometry, which is shown in Fig. 9.

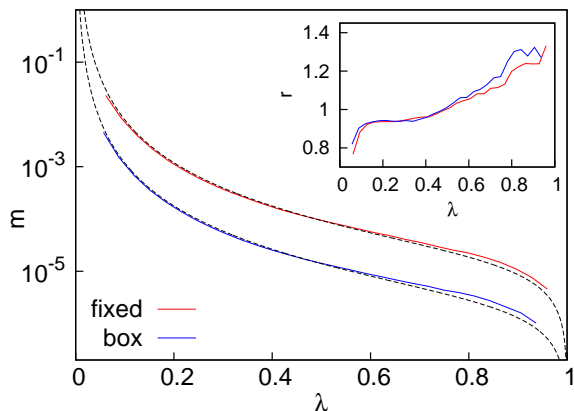


FIG. 9: (Color online) Magnetization profiles in 4D in the slab geometry for fixed-free b.c.-s in a system of width $L = 32$ for box- h and fixed- h randomness. The interpolation formula in Eq.(4) is represented by dashed lines. In the inset the ratio of the magnetization profile and the interpolation formula is shown for $x = 2.72$, $x_s = 3.7$, $A_{\text{fixed}} = 4.19$ and $A_{\text{box}} = 0.625$.

Close to the fixed surface the decay exponent is calculated as $x_b = 2.72(10)$, which agrees well with the finite-size estimate of the bulk magnetization exponent, see Table II. The magnetization profile close to the free

surface is shown in Fig. 10.

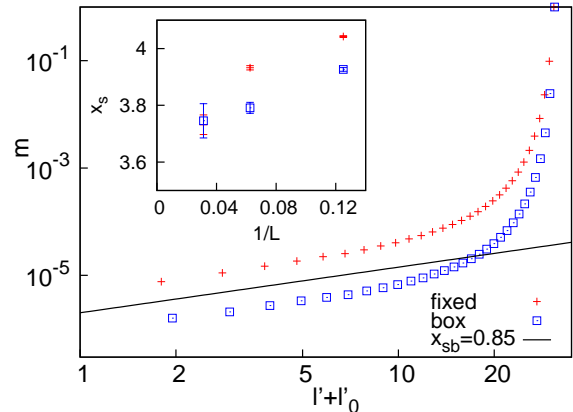


FIG. 10: (Color online) Magnetization profiles near the free boundary in 4D for the slab geometry for the two type of randomness with $L = 32$. In both cases the decay is characterized by the exponent, $x_{sb} = 0.85(15)$. In the inset the finite-size estimates for the surface magnetization exponent are presented. The extrapolated (disorder independent) value is given in Table II.

Estimates of the decay exponent, x_{sb} , and that of the surface magnetization exponent, x_s , which are presented in Table II contain somewhat larger errors, than in lower dimensional calculations. However the scaling relation in Eq.(3) is satisfied in this case, too. Also the interpolation formula in Eq.(4) is a good approximation as can be seen in the inset of Fig. 9.

IV. DISCUSSION

In this paper we have used the SDRG method to calculate the magnetization profiles of the random transverse Ising model in 2D, 3D and 4D in different geometries: slab, corner and wedge having a fixed surface. At the critical point decay exponents are calculated both at the fixed end and at the free end of the profiles. These exponents, which are presented in Table II are found to be disorder independent. From finite-size scaling studies of the local magnetization at the free ends of the profile local (surface, corner and edge) critical exponents are calculated, see Table II. For all types of profiles considered here the scaling relations in Eqs.(2) and (3) are satisfied and the interpolation formula in Eq.(4) is found to be a good approximation in the slab geometry. Our results, concerning the properties of the average local magnetization of the RTIM are rather complete, these are comparable with the existing results in the non-random system.

By the SDRG method the average local magnetization, m_l , is obtained as the ratio of such rare realizations, in which the correlation cluster contains the given site. By this method the typical value of the local magnetization could be estimated by the strength of the

effective coupling, J'_{1l} , which is generated between the fixed surface and the site. For surface spins it scales as $m_s^{typ} \sim J'_{1L} \sim \exp(-AL^\psi)$, where ψ is a characteristic exponent in the IDPF^{1,4}, which has been calculated in Refs.¹⁶⁻¹⁸. Thus by calculating m_s^{typ} by some other means one can obtain independent estimates for the exponent ψ .

Concerning the dimensional dependence of the average surface magnetization exponent, we write it in the form: $x_s(D) = D_s + p(D)$, where $D_s = D - 1$ is the dimension of the surface and $p(D)$ is a number close to $1/2$. In 1D $p(1) = 1/2$ is shown to be the persistence exponent of the random walk⁹ and we propose here an analogous explanation for $D > 1$, too. Let us denote by μ_s the number of surface points of the correlation cluster, \mathcal{C} which starts at the fixed boundary. We have checked, that μ_s has an exponential distribution: $P(\mu_s) \sim \exp(-\mu_s/\tilde{\mu})$, with $\tilde{\mu} \approx B(N/L)^{D-1}$, c.f. in 2D we have $B = 0.5$ and $B = 1.0$, for fixed- h and box- h disorder, respectively. Consequently the surface points of \mathcal{C} are grown from uncorrelated domains. The average number of surface points in an area L^{D-1} then scales as $[\mu_s]_{av} \sim L^{-p(D)}$.

TABLE II: Estimates of the critical exponents obtained by finite-size scaling: x , x_s , x_c , x_e and the exponents associated with the decay of the profile: x_b , x_{sb} , x_{cb} , x_{eb} . (x is taken from Refs.¹⁶⁻¹⁸ and the exact results in 1D are from Refs.^{3,5,9}).

	bulk		surface		corner		edge	
	x	x_b	x_s	x_{sb}	x_c	x_{cb}	x_e	x_{eb}
1D	$(3 - \sqrt{5})/4$		0.5					
2D	0.982(15)	0.98(1)	1.60(2)	0.65(2)	2.3(1)	1.35(10)		
3D	1.840(15)	1.855(20)	2.65(15)	0.84(7)	4.2(2)	2.65(25)	3.50(15)	1.75(15)
4D	2.72(12)	2.72(10)	3.7(1)	0.85(15)				

Our results about the local critical behavior of the RTIM are relevant to other random quantum magnets having discrete symmetry, we mention the random quantum Potts⁴¹, clock and Ashkin-Teller models⁴². Also the surface, corner and/or edge exponents of the random contact process are expected to be given by the RTIM values in Table II. To check this conjecture one should repeat recent Monte Carlo simulations about this model^{22,23}.

Our studies of the local critical behavior can be extended in different directions. For example, one can measure the corner and edge magnetization exponents at different opening angles or one can consider anisotropic sys-

As explained in Ref.¹⁸ (see Fig. 5 there) the correlation cluster is embedded into a connected subgraph, which contains all the decimated sites (the results of both h - and J -decimations) and which is related to a low-energy excitation of the system. The number of points in the connected subgraph is $\tilde{L} \sim L^{D_f}$, where the fractal dimension, D_f , is close to one. If we replace the connected subgraph with a linear chain with \tilde{L} sites then we obtain from the random walk result: $p(D) \approx D_f/2$. Indeed our numerical estimates¹⁹ of D_f and the surface magnetization scaling dimensions in Table II are in agreement with this relation. In higher dimensions we expect that the structure of the SDRG transformation, in particular the topology of the connected clusters follows the trend observed in this paper, thus the surface magnetization exponent generally obeys the relation: $x_s(D+1) - x_s(D) \approx 1$. Based on this result we expect that a simplified SDRG procedure, such as a modified version of those used in Refs.²⁵⁻³¹ can be constructed, which captures the main results about the surface critical properties of the RTIM.

tems, in which the distribution of disorder is different in the different directions. One can also consider the surface critical behavior in the presence of enhanced surface couplings, in which case the so called extraordinary and surface transitions³³⁻³⁵ could be studied, too.

Acknowledgments

This work has been supported by the Hungarian National Research Fund under grant No OTKA K75324 and K77629.

* Electronic address: kovacs.istvan@wigner.mta.hu

† Electronic address: igloi.ferenc@wigner.mta.hu

¹ For a review, see: F. Igloi and C. Monthus, Physics Reports

412, 277, (2005).

² S.K. Ma, C. Dasgupta and C.-K. Hu, Phys. Rev. Lett. **43**, 1434 (1979); C. Dasgupta and S.K. Ma, Phys. Rev. **B22**,

- 1305 (1980).
- ³ D.S. Fisher, Phys. Rev. Lett. **69**, 534 (1992); Phys. Rev. B **51**, 6411 (1995).
 - ⁴ D.S. Fisher, Physica A **263**, 222 (1999)
 - ⁵ B. M. McCoy and T. T. Wu, Phys. Rev. **176**, 631 (1968); Phys. Rev. **188**, 982 (1969); B. M. McCoy, Phys. Rev. **188**, 1014 (1969); Phys. Rev. B **2**, 2795 (1970).
 - ⁶ R. Shankar and G. Murthy, Phys. Rev. B **36**, 536 (1987).
 - ⁷ A. P. Young and H. Rieger, Phys. Rev. B **53**, 8486 (1996).
 - ⁸ F. Iglói and H. Rieger, Phys. Rev. Lett. **78**, 2473 (1997).
 - ⁹ F. Iglói and H. Rieger, Phys. Rev. **B57** 11404 (1998).
 - ¹⁰ O. Motrunich, S.-C. Mau, D.A. Huse and D.S. Fisher, Phys. Rev. B **61**, 1160 (2000).
 - ¹¹ Y.-C. Lin, N. Kawashima, F. Iglói and H. Rieger, Progress in Theor. Phys. **138**, (Suppl.) 479 (2000).
 - ¹² D. Karevski, Y-C. Lin, H. Rieger, N. Kawashima and F. Iglói, Eur. Phys. J. B **20** 267 (2001).
 - ¹³ Y-C.Lin, F. Iglói and H. Rieger, Phys. Rev. Lett. **99**, 147202 (2007).
 - ¹⁴ R. Yu, H. Saleur and S. Haas, Phys. Rev. B **77**, 140402 (2008).
 - ¹⁵ I. A. Kovács and F. Iglói, Phys. Rev. B **80**, 214416 (2009).
 - ¹⁶ I. A. Kovács and F. Iglói, Phys. Rev. B **82**, 054437 (2010).
 - ¹⁷ I. A. Kovács and F. Iglói, Phys. Rev. B **83**, 174207 (2011).
 - ¹⁸ I. A. Kovács and F. Iglói, J. Phys. Condens. Matter **23**, 404204 (2011).
 - ¹⁹ I. A. Kovács, PhD thesis (2012).
 - ²⁰ I. A. Kovács and F. Iglói, EPL **97**, 67009 (2012).
 - ²¹ C. Pich, A.P. Young, H. Rieger and N. Kawashima, Phys. Rev. Lett. **81**, 5916 (1998).
 - ²² T. Vojta, A. Farquhar and J. Mast, Phys. Rev. E **79**, 011111 (2009).
 - ²³ T. Vojta, arXiv:1209.1400 (2012).
 - ²⁴ J. Hooyberghs, F. Iglói and C. Vanderzande, Phys. Rev. Lett. **90** 100601, (2003); Phys. Rev. E **69**, 066140 (2004).
 - ²⁵ O. Dimitrova and M. Mézard, J. Stat. Mech. P01020 (2011).
 - ²⁶ C. Monthus and Th. Garel, J. Phys. A: Math. Theor. **45**, 095002 (2012).
 - ²⁷ C. Monthus and Th. Garel, J. Stat. Mech. P01008 (2012).
 - ²⁸ C. Monthus and Th. Garel, J. Stat. Mech. P05002 (2012).
 - ²⁹ C. Monthus and Th. Garel, J. Stat. Mech. P10010 (2012).
 - ³⁰ C. Monthus and Th. Garel, J. Stat. Mech. P09016 (2012).
 - ³¹ R. Miyazaki and H. Nishimori, arXiv:1210.5053 (2012).
 - ³² L. B. Ioffe and M. Mézard, Phys. Rev. Lett. **105**, 037001 (2010); F. M. Feigel'man, L. B. Ioffe and M. Mézard, Phys. Rev. B **82**, 184534 (2010).
 - ³³ K. Binder, in *Phase Transitions and Critical Phenomena*, edited by C. Domb and J. L. Lebowitz (Academic, London, 1983), Vol. 8, p. 1.
 - ³⁴ H. W. Diehl in *Phase Transitions and Critical Phenomena*, edited by C. Domb and J. L. Lebowitz (Academic Press, London, 1986), Vol. 10, p. 75.
 - ³⁵ M. Pleimling, J. Phys. A **37**, R79 (2004).
 - ³⁶ C. Monthus, Phys. Rev. B **69**, 054431 (2004)
 - ³⁷ F. Iglói, I. Peschel, and L. Turban, Advances in Physics **42**, 683 (1993).
 - ³⁸ M.E. Fisher, and P-G. de Gennes, C. R. Acad. Sci. (Paris) **287**, 207 (1978).
 - ³⁹ T. W. Burkhardt and T. Xue, Phys. Rev. Lett. **66**, 895 (1991).
 - ⁴⁰ M. Karsai, I. A. Kovács, J-Ch. Angles d'Auriac and F. Iglói Phys. Rev. E **78**, 061109 (2008).
 - ⁴¹ T. Senthil and S. N. Majumdar Phys. Rev. Lett. **76**, 3001 (1996)
 - ⁴² E. Carlon, P. Lajkó, and F. Iglói, Phys. Rev. Lett. **87**, 277201 (2001)